Highlights

Investigation of recombination mechanisms in Cu(In,Ga)Se_2 solar cells using numerical modelling

Sheng Yang,Samira Khelifi,Jessica de Wild,Bart Vermang,Johan Lauwaert

- Surface, interface and bulk recombination mechanisms in CIGSe thin-film solar cells are distinguished by numerical modelling and regression analysis based on the solar cell performance.
- Global optimization algorithm differential evolution is used in the regression analysis to avoid finding local minimal of the cost function. Good algorithmic performance and a convincing global minimization are obtained in the fitting process.
- The recombination mechanisms are found to be different in solar cells with different preparation methods and absorber thickness. For CIGSe solar cells with a relatively thick absorber layer, the main loss is found to be the bulk recombination through deep level defects. For cells with an ultra-thin absorber layer, the back surface recombination is found to be the main loss mechanism. Based on the proposed numerical model and the observed loss mechanisms, suggestions are given for further improving the solar cell efficiency in each cell.

Investigation of recombination mechanisms in Cu(In,Ga)Se_2 solar cells using numerical modelling

Sheng Yang[a], Samira Khelifi[b], Jessica de Wild[c,d,e], Bart Vermang[c,d,e] and Johan Lauwaert[a]

[a] *Department of Electronics and Information Systems, Ghent University, Technologiepark 126, 9052 Zwijnaarde, Belgium*
[b] *Department of Solid State Sciences, Ghent University, Krijgslaan 281/S1, B-9000 Gent, Belgium*
[c] *Institute for Material Research (IMO), Hasselt University (partner in Solliance), Agoralaan gebouw H, Diepenbeek, 3590, Belgium*
[d] *EnergyVille, Thor Park 8320, 3600 Genk, Belgium*
[e] *Imec division IMOMEC (partner in Solliance), Wetenschapspark 1, 3590 Diepenbeek, Belgium*

ARTICLE INFO

Keywords:
CIGSe solar cell
Recombination mechanisms
Numerical modelling
Regression analysis
Differantial evolution

ABSTRACT

In this work, recombination mechanisms are investigated in Cu(In, Ga)Se_2 solar cells based on numerical modelling and verified by regression analysis of the dark and light current density-voltage (J-V) curves. Loss mechanisms such as a back contact barrier, deep level defects in the absorber layer are determined by fitting the simulated cell performance with the measurements using global optimisation algorithm differential evolution. The cell performance in the fitting process includes J-V curves recorded at different temperatures and open-circuit voltage(V_{oc}) under different illumination intensities at 300K. The results show that for CIGSe solar cells with different preparation methods and absorber thickness, the main loss mechanisms are different. Based on the proposed numerical model and the observed loss mechanisms, suggestions are given for further improving the solar cell efficiency in each cell.

1. Introduction

Thin-film solar cells with Cu(In, Ga)(S, $Se)_2$ (CIGSe) absorber have achieved an efficiency of 23.35% which is one of the highest efficiencies recorded in thin-film solar cell technology [1]. However, defects in the CIGSe absorbers and their influence on the cell performance is still far from being well understood.

Characterization of the defects in the absorber layer is currently done through techniques such as Admittance Spectroscopy (AS) [2] and Deep Level Transient Spectroscopy (DLTS) [3]. They have the disadvantage that the signals are influenced by parasitic effects induced by the complex layer structure. As a result, the low-temperature signal (N1) that occurs independently of the preparation methods was questioned for a long time [4, 5, 6, 7, 8]. The room temperature signal(N2) is attributed to a recombination center and has been associated with V_{oc} losses[9, 10]. However, photoconductive measurements show that at least 11 other components are present in addition to the N1 and N2 signal[11]. An alternative optical technique for the detection of shallow defect levels is, for example, photoluminescence (PL)[12]. These optical techniques are not influenced by parasitic effects but have the disadvantage that they do not provide direct information on the carrier capture cross-sections of the defects.

Theoretically, density functional theory (DFT) calculations within the local density approximation[13, 14] and with hybrid exchange-correlation functionals[15, 16, 17, 18, 19] are applied to $CuInSe_2$ and $CuGaSe_2$. There are contradictory results on whether Cu_{In}, In_{Cu} are shallow or deep defects that cause recombination losses[13, 15, 18]. Cu_{Ga} and Ga_{Cu} are found to be deep traps from theoretical calculation, however, experimentally Ga_{Cu} defect is found to be a shallow defect from photoluminescence spectroscopy[20].

As discussed above, although many intrinsic defects have already been observed both theoretically and experimentally, the knowledge on the defects present in these compounds is still incomplete. Distinguishing among surface, interface and bulk recombination is also a big challenge in thin-film solar cells. Due to the incomplete knowledge, it is not straightforward to demonstrate how the observed defects and the recombination mechanism influence the solar cell performance while this is very valuable information to support the further improvement of the solar cell efficiency.

In this work, we show that different recombination mechanisms and defects properties influence solar cell performance in distinctive ways. By analyzing the measured performance data including temperature and illumination dependent current density-voltage(J-V) curve and open-circuit voltage(V_{oc}), we build numerical models for CIGSe

ORCID(s):

solar cells and determine the defects and recombination related model parameters with regression analysis. The conventional fitting methods used in regression analysis based on gradient search can easily be stuck at the local minimum of the cost function. To obtain a more conclusive fitting result, the intelligence global optimisation algorithm differential evolution is used in building the model. This modelling method is applied to three CIGSe solar cells with different preparation methods and absorber thickness. The main recombination mechanisms in those samples are verified by the regression analysis and are found to be different in the three cells.

The paper is structured as follows: Section 2 gives the basic information on the three CIGSe samples under investigation. Section 3 analyzes the failure in light/dark superposition of the J-V curves and V_{oc} deficit for CIGSe solar cells and the method of how we can investigate the recombination mechanisms based on the J-V curves. Section 4 explains the detailed process of modelling and regression analysis using one sample as a demonstration. Then the results of the fitting and the proposed numerical models for all three samples are given. In the end, Section 5 discusses the model parameters and the discovered recombination mechanisms in the CIGSe solar cells.

2. Solar cells under investigation

Three CIGSe solar cells labeled as S1600, S1000 and S430 were investigated. The absorber's thickness w of samples S1600, S1000 and S430 are 1600 nm, 1000 nm, 430 nm respectively. The bandgaps of these cells are 0.99 eV, 1.13 eV, 1.18 eV respectively.

The samples S430 and S1000 were prepared by a one-stage co-evaporation deposition at Solliance. The CIGSe layers are deposited on Mo/Si(O,N)/ soda-lime glass substrate(SLG). The Si(O,N) layer acts as an alkali barrier layer. For S1000, before the CIGSe growth, 5nm NaF was evaporated on the substrate. During the evaporation process, the four elements Cu, In, Ga, Se are heated separately in different crucibles with different temperatures, then all of them are simultaneously evaporated onto the heated substrate(550 $°C$). The Cu/(Ga+In) ratio(CGI) and Ga/(Ga+In) ratio(GGI) for S1000 is 0.79/0.26(CGI/GGI). The CGI/GGI in S430 is 0.86/0.31. For S430, there is no NaF treatment, but a KF spin-coating was performed after the growth of the CIGSe absorber layer[21].

Sample S1600 was prepared by a two-step process[22]. The CIGSe absorber layer was made from electrodeposited metal layers followed by selenization. The substrate for S1600 is SLG/Mo without the Si(O,N) alkali barrier layer. The CGI/GGI in S1600 is about 0.85/0.30. However, in CIGSe solar cells prepared by such a two-step process, Ga accumulation is often found at the back contact[23, 24]. This results in a low GGI ratio around the space charge region and a reduction of the bandgap energy there. In S1600, the bandgap is measured to be 0.99eV which is lower than the bandgap of the other two samples.

The schematic of the CIGSe solar cells is shown in Figure 1.

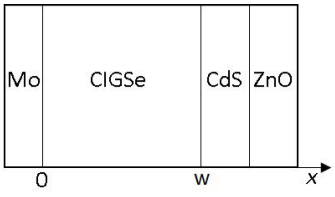

Figure 1: Schematic of the CIGSe solar cell

The performance of the three solar cells: open circuit voltage(V_{oc}), short circuit current(J_{sc}), efficiency(η), fill factor(FF) are shown in Table 1.

3. Method

We start the investigation of the recombination mechanisms, defects properties and possible losses in the solar cell by analyzing the solar cell performance. Given sample S1600 as an example: The J-V curves of the S1600 measured in dark and illumination under standard conditions (300K and A.M 1.5) are shown in Figure 2.

Sample	CGI	GGI	Eg(eV)	V_{oc}(mV)	J_{sc}(mA/cm^2)	η(%)	FF(%)
S1600	0.85	0.30	0.99	595.8	36.2	13.6	62.3
S1000	0.79	0.26	1.13	543.7	25.1	8.1	59.0
S430	0.86	0.31	1.18	576.2	18.9	7.1	64.7

Table 1
Chemical composition, bandgap of the absorber layers and solar cells parameters measured under standard conditions (300K and A.M 1.5)

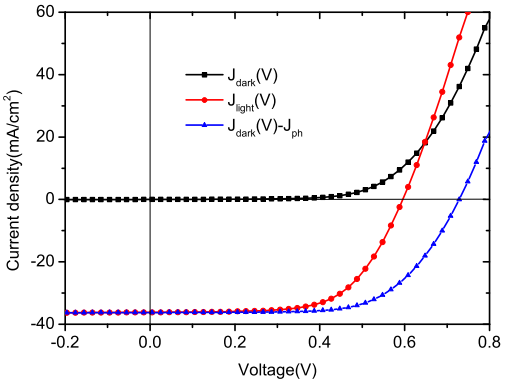

Figure 2: J-V curves of the S1600. $J_{dark}(V)$: J-V curve of the S1600 Measured in dark; $J_{light}(V)$: J-V curve of the S1600 measured in illumination under standard conditions (300K and A.M 1.5); $J_{dark}(V) - J_{ph}$: Measured dark current plus the short circuit current under illumination.

The ideal current density of a p-n junction is given by

$$J_L = J_s(exp(\frac{qV}{nkT}) - 1) - J_{ph} \tag{1}$$

where J_s is the saturation current density, V is the applied voltage, q is the elementary charge, k is the Boltzmann's constant, T is temperature, and n is the ideality factor, J_{ph} is the photogenerated current density. If the cell performance of S1600 follows the ideal current density equation, the light current of S1600 should be the $J_{dark}(V) - J_{ph}$ in Figure 2. However, as we can see from Figure 2 curve $J_{light}(V)$ and $J_{dark}(V) - J_{ph}$, the J-V curve under illumination doesn't follow the superposition of dark current and photogenerated current under the forward bias, there is a V_{oc} deficit for the measured J-V curve. The V_{oc} deficit is commonly observed in CIGS solar cells[25, 26]. This implies that under illumination the forward bias diffusion current is higher than in the dark condition so it compensates more for the photogenerated current than expected. The forward bias diffusion current is dependent on the recombination. There are three main recombination mechanisms in the solar cell:

- Recombination in the bulk of the CIGSe absorber.

The Shockley-Read-Hall(SRH) recombination current in the bulk of CIGSe absorber is given by Equation 2.

$$J_{Rbulk} = \int_0^w U(x)dx = \int_0^w \frac{n(x)p(x) - n_i^2}{\tau_p[p(x) + n_i e^{(E_i - E_t)/kT}] + \tau_n[n(x) + n_i e^{(E_t - E_i)/kT}]} dx \tag{2}$$

where $U(x)$ is the SRH recombination rate[27], w is the thickness of the CIGSe absorber layer. n and p are the carrier density for electrons and holes respectively. n_i is the intrinsic electron density. τ_n and τ_p are the carrier lifetimes for electrons and holes respectively linked to the defects by $\tau_{n/p} = 1/\sigma_{n/p} v_{th} N_t$ with σ_n and σ_p the electron and hole capture cross-sections respectively, v_{th} the thermal velocity, N_t the defect density. E_i is the intrinsic Fermi level and E_t is the defect energy level.

- Recombination between the buffer and the absorber layer.

Recombination at the interface between the CIGSe absorber and the CdS buffer layer which results in a recombination current J_{Rif}. The SRH recombination process is similar as in the bulk of the CIGSe absorber layer, however here the capture and emission of charge carriers are considered from both sides of the CdS/CIGSe interface.

- Recombination at the back contact surface.

The back surface recombination current is given by Equation 3.

$$\begin{aligned} J_{Rback} &= qS_n[n(0) - n_{back}] \\ n_{back} &= N_c exp(\Phi_b/kT) \end{aligned} \tag{3}$$

where S_n is the back surface recombination velocity for electrons, n_{back} is the thermal equilibrium density of electrons at the back contact, N_c is the density of states in the conduction band in the CIGSe absorber layer, Φ_b is the corresponding back contact injection barrier.

As discussed above, these three recombination mechanisms contribute to the overall recombination current in different forms. Thus, in the regression analysis, the three recombination mechanisms and the defects properties can be regarded as the set of unknown model parameters β, the applied voltage and illumination are the independent variables X and the output current and solar cell performance parameters are the dependent variable $Y = f(X, \beta)$. By estimating the function $f(X, \beta)$ that most closely fits the cell performance measurements data (IV curve, V_{oc}, J_{sc}, η, FF), the unknown model parameters β can be determined.

4. Experimental

4.1. Numerical modelling

To start the regression analysis of the model parameters β, we first have to specify the form of the function f. CIGSe thin-film solar cells consist of several layers with different materials. They form a heterojunction with band discontinuities and interface states. For these solar cells with complicated structure, the assumptions and simplifications that are needed in order to construct an analytical model may not be applicable anymore. The analytical expression given by Equation 1 for J-V curves often can not explain the crossover and rollover phenomenon observed in these thin-film solar cells[28, 29]. Thus, a numerical model which can describe the complicated layered structure is necessary for these devices. There are several commonly used software that can perform numerical simulation for thin-film solar cells such as SCAPS[30], PC-1D[31], Sentaurus TCAD[32]. However, there are often no powerful fitting tools embedded in them for regression analysis. In our case, for the multi-variable optimization problem, adapting the parameters manually to get a good fitting can be very time-consuming and difficult to ensure a global optimal. In this work, we use our in house software 'FFmachine' to build the numerical model[33]. This solves the semiconductor equations in an equivalent way as in SCAPS but includes a powerful fitting tool to support building the model. FFmachine is written in Fortran95 and it obtains a one-dimensional solution for van Roosbroeck system, which consists of three nonlinear ordinary differential equations for the unknown electrostatic potential $\Phi(x)$, the quasi Fermi potential for electrons $\phi_n(x)$ and the quasi Fermi potential for holes $\phi_p(x)$.

$$\begin{aligned} \frac{\partial^2\Phi}{\partial x^2} &= \frac{q}{\epsilon\epsilon_0}[n(\Phi,\phi_n) - p(\Phi,\phi_p) - N_D^+ + N_A^- - \frac{\rho_{defect}}{q}] \\ \frac{\partial J_n}{q\partial x} &+ G - U(\Phi,\phi_n) = 0 \\ \frac{\partial J_p}{q\partial x} &- G + U(\Phi,\phi_p) = 0 \end{aligned} \tag{4}$$

Where ϵ is the dielectric constant and ϵ_0 is the permittivity of the free space. N_D^+ and N_A^- are the density of ionized donors and acceptors respectively, $\rho_{defect}(x)$ is the charge density of the defect states. G is the rate of generation, U is the recombination rate given by $qU = J_{Rbulk} + J_{Rif} + J_{Rback}$. J_n and J_p are the electron and hole current densities respectively.

$$\begin{aligned} J_n &= -q\mu_n n(\Phi,\phi_n)\frac{\partial\phi_n}{\partial x} \\ J_p &= -q\mu_p p(\Phi,\phi_p)\frac{\partial\phi_p}{\partial x} \end{aligned} \tag{5}$$

μ_n and μ_p are the free electron and hole mobilities ($cm^2\ V^{-1}\ s^{-1}$), the electron density n and the hole density p are related to the electric potential Φ as well as the quasi Fermi potentials of electrons and holes via

$$\begin{aligned} n(\Phi, \phi_n) &= N_c exp[\frac{q(\Phi - \phi_n) - E_c}{k_B T}] \\ p(\Phi, \phi_p) &= N_v exp[\frac{q(\phi_p - \Phi) + E_v}{k_B T}] \end{aligned} \tag{6}$$

In the literature, these carrier densities n and p are often set as unknowns for the van Roosbroeck system [33, 34, 35]. However, here we upgraded our software to solve this system of equation for the quasi-fermi potentials[36]. Therefore this solver follows an equivalent methodology as the one used in SCAPS-1D [30].

By numerically solving the van Roosbroeck system, the carrier distributions under different applied voltages are obtained. The output current of the solar cell, η, V_{oc}, J_{sc}, FF are calculated accordingly.

4.2. Regression analysis

After having constructed the model form $Y = f(X, \beta)$. Regression analysis of the unknown model parameters can be implemented by fitting simulated solar cells performances to the measurements.

The basic parameters in the model for S1600 are shown in Table 2. The bandgap of the CIGSe layer is determined by linear extrapolation of the long wavelength slope in the EQE plots. The thickness of the absorber is determined with X-ray Fluorescence Spectrometer(XRF) and Scanning Electron Microscope(SEM). The electron affinity of the layers are taken from reference[37]. The parameters marked with (f) in Table 2 are those to be determined by regression analysis, and their values are given in a range during the fitting process. Here the doping density is also set as a fitting parameter because the U-shaped doping profiles are commonly found in CIGS absorber by capacitance-voltage (C-V) profiling [38]. There are contradicting views on whether that can be attributed to a real spatial variation in doping or if it is an artifact caused by the presence of certain defect levels and a back contact barrier [39, 40, 41]. Interpreting the actual doping profile from the apparent U-shape doping profile is a matter of debate [42]. The absorption coefficient is calculated using Equation 7. The carriers mobility in ZnO and CdS are taken from reference[43]. Other parameters in the table are taken from literature [44].

$$\alpha(\lambda) = (A + \frac{B}{h\upsilon})\sqrt{h\upsilon - E_g} \tag{7}$$

Where E_g is the band gap of the material, A (in $cm^{-1}eV^{-1/2}$) and B (in $cm^{-1}eV^{-1/2}$) are the model constants.

To distinguish the influence of each recombination mechanism on the solar cell performance, not all the unknown parameters are fitted simultaneously. Instead, when the effect of one parameter is investigated, other unknown parameters are controlled. We did four independent rounds of regression tests with different β arrays that including defects in different positions in the cell as shown in Table 3.

-In the first regression test: it is assumed that there is only a back contact barrier, no defects present in the solar cell.

-In the second regression test: the defects are assumed to be only present at the interface between the CIGSe absorber layer and the CdS buffer layer.

-In the third regression test: the defects are assumed to be present only in the buffer layer.

-In the fourth regression test: the defects are only present in the CIGSe absorber layer.

The range of parameters in the fitting process is shown in Table3. The defects are assumed to be uniformly distributed.

4.3. Fitting process

The performance used in the fitting process are dark and light J-V curves and V_{oc} under different light intensities at 300K. The J-V measurements are carried out using a source Measure Unit (KEITHLEY 2600B). A Xenon arc lamp(Model Oriel 6143) together with neutral density filters ranging from 0 to 100 mW/cm^2 are used to mimic different illumination intensities of the sunlight.

Parameters	ZnO	CdS	CIGSe(S1600)
Thickness (nm)	50	50	1600
Bandgap (eV)	3.3	2.4	0.99
Electron affinity (eV)	4.4	4.2	4.5
Dielectric permittivity (relative)	9	10	13.6
Electron mobility($cm^2/V.s$)	200	350	100
Hole mobility($cm^2/V.s$)	50	50	25
Shallow uniform acceptor density,$N_A(1/cm^3)$	1	1	5.83×10^{14} to 1.17×10^{16} (f)
Shallow uniform donor density,$N_D(1/cm^3)$	1×10^{18}	1×10^{18}	10
Absorption model parameter A($cm^{-1}eV^{-1/2}$)	1×10^5	1×10^5	1×10^3 to 1×10^5 (f)
Absorption model parameter B($cm^{-1}eV^{-1/2}$)	0.001		
CB effective density of states($1/cm^3$)	2.2×10^{18}		
VB effective density of states($1/cm^3$)	1.8×10^{18}		
Electron thermal velocity(cm/s)	1×10^7		
Hole thermal velocity(cm/s)	1×10^7		
Back contact metal work function (eV)	4.5 to 6.5 (f)		
Back surface recombination velocity for electron (cm/s)	1×10^7		
Back surface recombination velocity for holes (cm/s)	1×10^7		
Series resistance($Ohm.cm^2$)	0.1 to 20 (f)		
Shunt resistance($Ohm.cm^2$)	1 to 1000 (f)		

Table 2
Parameters in the numerical model for S1600. The parameters marked with (f) are set as variables in the fitting process.

R	Defects position	$\sigma_{e/h}(cm^2)$	E_t above E_i(eV)	N_t
1	-	-	-	-
2	Interface	3.14×10^{-17} to 4.66×10^{-15}	−0.4 to 0.4	4.86×10^8 to 1.19×10^{11} $(1/cm^2)$
3	Buffer	3.14×10^{-17} to 1.39×10^{-11}	−0.4 to 0.4	1.43×10^{17} to 1.74×10^{18} $(1/cm^3)$
4	Absorber	3.14×10^{-17} to 1.39×10^{-11}	−0.4 to 0.4	7.90×10^{13} to 2.35×10^{17} $(1/cm^3)$

Table 3
The range for the fitting parameters in the four-round of variable controlled regression analysis: R is the number of the regression test; $\sigma_{e/h}$ are the defects capture cross sections for electrons/holes; E_t is the energy level of the defects; E_i is the intrinsic Fermi level; N_t is the defects density.

In the fitting process, the cost function CF to be minimized is defined as shown in Equation 8.

$$\begin{aligned} CF &= CF(JV) + CF(V_{oc}) \\ CF(JV) &= \sum_{i=2}^{N-1} d^2\{(V_i, J_{model}(V_i)), l[(V_{i-1}, J_{meas}(V_{i-1})), (V_{i+1}, J_{meas}(V_{i+1}))]\}/(N-2) \\ CF(V_{oc}) &= \sum_{j=1}^{M} [V_{oc}(e)_j - V_{oc}(s)_j]^2/M \end{aligned} \tag{8}$$

$CF(JV)$ is the difference of the J-V curves between simulation and measurement. $CF(V_{oc})$ is the V_{oc} difference between simulation and measurements. N is the number of points in the J-V measurements. (V_i,$J_{model}(V_i)$) is the coordinate of a point in the simulated J-V curve. l is the line formed by the two measurement points(V_{i-1},$J_{meas}(V_{i-1})$) and (V_{i+1},$J_{meas}(V_{i+1})$). d is the distance between line l and the point (V_i,$J_{model}(V_i)$). The distance d is used to normalize the current values, because the current values in logarithm or exponential form have extreme values that dominate the cost function and produce a biased fitting result. M is the number of V_{oc} measured at 300K under different light intensities. V_{oc}(e) is experimentally measured V_{oc} value, V_{oc}(s) is simulated V_{oc} value. V_{oc} values in function of illumination are especially included in the cost function because it is closely related to the recombination current.

Adapting manually the independent parameters to reach a good fitting strongly rely on the experience of the scientist and can cost a lot of time. Using the traditional curve fitting methods based on the gradient search can easily

be stuck at the local minimum of the cost function. Thus, here we use a global optimization algorithm differential evolution[45] from the Scipy package of Python. Differential evolution as a stochastic global optimisation algorithm has the advantages of the ability to locate the global optimum regardless of the initial values, it also has relatively fast convergence and it uses few control parameters[46].

In this work, the fitting process is carried out with a python script. Figure 3 shows the flow chart of the fitting process.

To start the fitting process, an initial population with $NP = 15 \times (number\ of\ unknown\ parameters)$ individuals is created. Each individual is a vector x with the unknown parameters as the elements. The value of these elements is randomly defined within the range given in Table 2 and 3.

Then the population goes through a mutation: For each vector(individual) $x_i (i \in [1, NP])$ in the population, three other vectors(x_{r1}, x_{r2}, x_{r3}) are randomly selected to generate the mutant vector which is also called donor vector v_i. $v_i = x_{r1} + F(x_{r2} - x_{r3})$ where F is the mutation scaling factor randomly chosen from the range[0.5,1).

The donor vector v_i then exchanges some elements with the original vector x_i to generate a new trial vector u_i in the recombination process. Whether the elements in v_i are exchanged with x_i depends on the control parameter called crossover probability, here we set it as 0.7. A random number $rand$ is generated for each elements, if $rand < 0.7$, then that element in v_i is exchanged with the corresponding elements in x_i, The new v_i is regarded as the trial vector u_i.

Now in the population, each individual x_i has a corresponding trial vector u_i, to compare which set of parameters are better, the cost function CF needs to be calculated. To get the value of CF, the Fortran routine is called to calculate the values for $J_{model}(V)$. The cost function includes J-V and V_{oc} differences at 16 different illuminations from 0 to $100 mW/cm^2$. To speed up the computation, 16 cores in the High-performance computer(VSC) are used to solve the van Roosbroeck system under different illuminations in parallel with OpenMP[47].

The Fortran calculated $J_{model}(V)$ is then sent back to python to calculate the cost function $CF(x_i)$ and $CF(u_i)$. The better individual from x_i and u_i will remain in the population. This process will be repeated until all the individuals in the population are very similar to each other with a standard error smaller than 0.1. The best individual from the final population is taken as the optimised set of parameters.

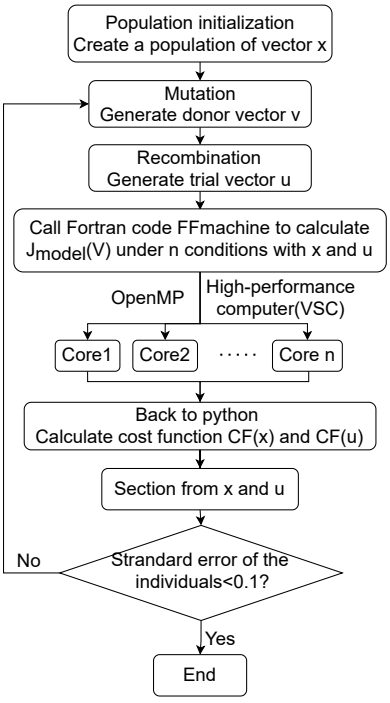

Figure 3: Flow chart of the fitting process

R	1	2	3	4
A	8679.51	8577.13	8577.18	8522.43
$N_A(1/\text{cm}^3)$	5.22×10^{15}	5.94×10^{15}	2.46×10^{15}	8.56×10^{15}
W_b(eV)	5.52	5.53	5.52	5.58
R_s (Ohm.cm^2)	4.07	3.87	1.37	3.25
Rsh (Ohm.cm^2)	1778.10	1717.32	1753.97	2609.85
Defects position	-	Interface	Buffer	Absorber
N_t	-	$6.69\times10^{10}(1/\text{cm}^2)$	$2.05\times10^{17}(1/\text{cm}^3)$	$1.06\times10^{14}(1/\text{cm}^3)$
E_t above E_i(eV)	-	-0.14	-0.27	0.09
$\sigma_e(\text{cm}^2)$	-	1.22×10^{-15}	8.05×10^{-15}	8.08×10^{-17}
$\sigma_h(\text{cm}^2)$	-	1.19×10^{-15}	1.50×10^{-14}	1.16×10^{-11}

Table 4
Parameters in the numerical model after the fitting in the four regression tests for S1600: R is the number of the test; A is the absorption model constant; N_A is the shallow uniform acceptor density; W_b is the back contact metal work function; $\sigma_{e/h}$ are the defects capture cross sections for electrons/holes; E_t is the energy level of the defects; E_i is the intrinsic Fermi level; N_t is the defects density.

4.4. Fitting results

Due to the stochastic nature of the differential evolution optimisation algorithm, the fitting process is performed 20 times and the best set of parameters is taken for the model shown in Table 4. The dark and light J-V curves and V_{oc} as a function of illumination calculated with the optimised model are shown in Figure 4 and Figure 5. During the 20 runs in each of the four tests, the minimal value of the cost function CF_{min} and the maximal value of the cost function CF_{max} all satisfy the relation $CF_{min} > (1-10\%)CF_{mean}$ and $CF_{max} < (1+10\%)CF_{mean}$ where CF_{mean} is the average value for CF in 20 runs. This implies a good algorithmic performance and a convincing global minimal of the fitting process.

4.4.1. Influence of the back barrier and interface defects

Comparing the first and the second regression test R1 and R2, the model difference is that in the second test interface defects are added. However, as shown in Figure 4(a) and (b), by adding interface defects, the IV curves show similar behavior as in the first test(without interface defects present). This indicates that the interface defects have a small influence on the solar cell performance while the back barrier is dominating the cell performance. In addition, with only back barrier and interface defects, the model can not match the measurement well.

4.4.2. Influence of defects in the buffer layer

In the third test, only defects in the buffer layer are added in the model. As shown in Figure 4(c), the defect in the buffer layer can lead to a crossover phenomenon in the IV curves. In some literature[29, 48], the proposed explanation is that a secondary barrier results from the conduction band offset between CIGS and the commonly used CdS buffer layer. This barrier produces a second diode with the same polarity and in series with the primary photodiode. The secondary-diode barrier height is modified by photoinduced changes of trap occupancy in the CdS layer, hence creating a voltage shift between dark and light conditions[28].

4.4.3. Influence of defects in the absorber layer

In the fourth regression test, a single level defect in the bulk of the CIGSe layer is implemented in the model, as shown in Figure 4(d) and Figure 5, with the bulk defects, the light IV curve and V_{oc}(illumination) have a better correspondence with the measurements, which indicates that bulk defects have a large influence on the solar cell performance.

From the four tests, it is verified that the recombination at different positions contributes differently to the solar cell performance. Interface defects have a small influence while the bulk defects have a strong impact on the loss. The same regression tests are performed on the other two samples S1000, S430 using the same parameter settings in Table 2 and Table 3 except for the different thickness and bandgap of the absorber layer. S1000 shows similar behavior as S1600 that defects in both CdS and CIGSe layer need to be included in the model for a good fitting. For S430, it is found that the back barrier has an important effect on the solar cell performance while the impact of the defects is limited.

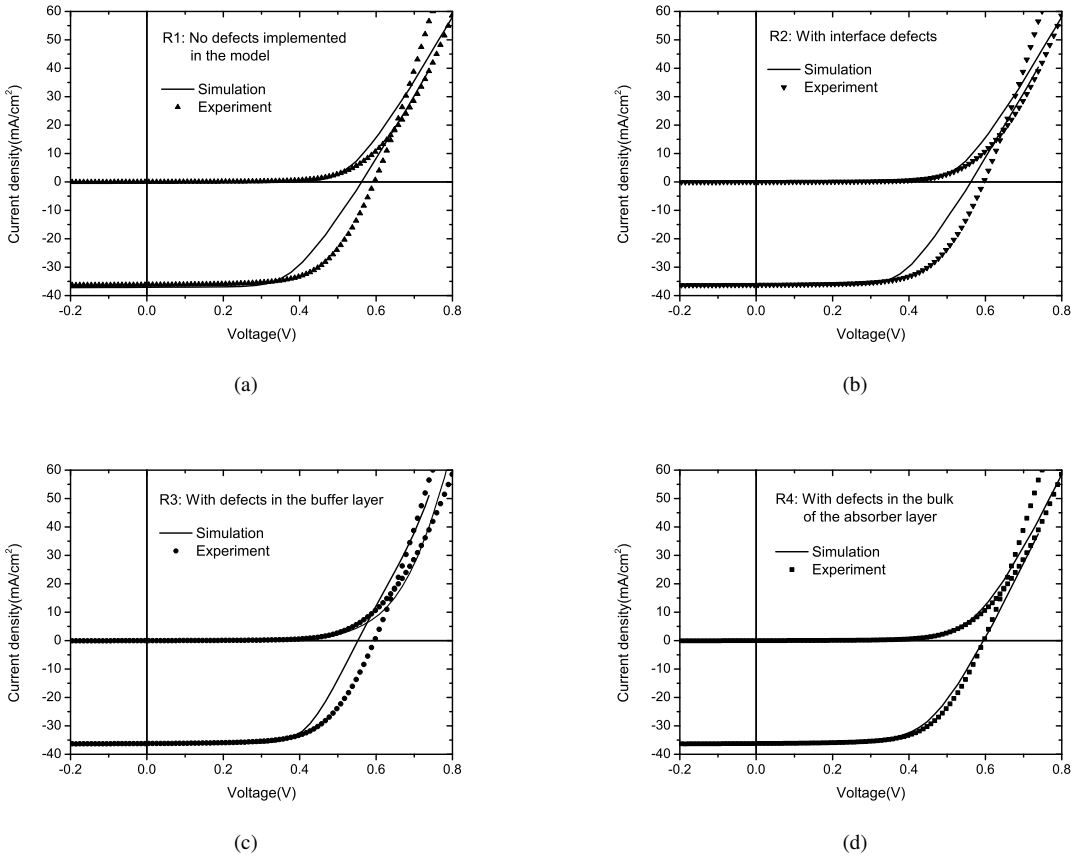

Figure 4: Dark and Light IV curves at 300K for S1600 in the 4 rounds of regression analysis: (a)R1: No defects present in the model; (b)R2: Defects only present in the interface of CdS and CIGSe layer of the model; (c)R3: Defects only present in the CdS layer of the model; (d)R4: Defects only present in the CIGSe layer of the model

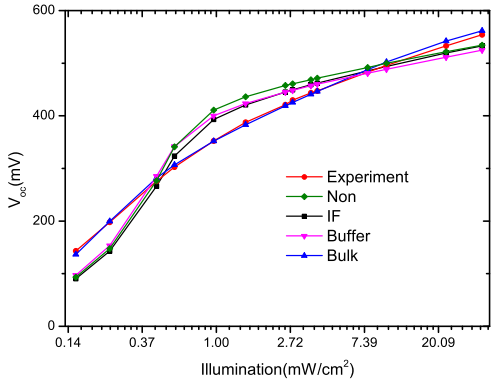

Figure 5: V_{oc} as a function of illumination at 300K for S1600: Non(no defects present in the model), IF(defects only present in the interface of CdS and CIGSe layer of the model); Buffer(defects only present in the CdS layer of the model); Bulk(defects only present in the CIGSe layer of the model)

		S1600	S1000	S430
CIGSe	A	7826.22	19388.44	14163.74
CIGSe	$N_A(1/\text{cm}^3)$	6.06×10^{14}	3.06×10^{15}	6.69×10^{15}
Defects in CIGSe layer	N_t $(1/\text{cm}^3)$	9.67×10^{14}	3.18×10^{16}	-
	E_t above E_i(eV)	0.14	0.11	-
	$\sigma_e(\text{cm}^2)$	3.25×10^{-17}	7.26×10^{-16}	-
	$\sigma_h(\text{cm}^2)$	2.26×10^{-14}	6.32×10^{-17}	-
Defects in CdS layer	N_t $(1/\text{cm}^3)$	1.97×10^{17}	1.27×10^{17}	-
	E_t above E_i(eV)	-0.18	0.27	-
	$\sigma_e(\text{cm}^2)$	1.62×10^{-16}	6.99×10^{-17}	-
	$\sigma_h(\text{cm}^2)$	6.48×10^{-15}	1.29×10^{-15}	-
Back contact	metal work function (eV)	5.61	5.24	5.42
	Barrier for holes (eV)	-0.39	0.17	0.05
Series resistance	(Ohm.cm^2)	1.86	1.65	1.84
Shunt resistance	(Ohm.cm^2)	2793.52	7604.89	624.8

Table 5
Parameters in the numerical model after fitting for S430, S1000 and S1600: A is the absorption model constant; N_A is the shallow uniform acceptor density; N_t is the defect density; E_t is the energy level; $\sigma_{e/h}$ are the defects capture cross sections for electrons/holes.

4.5. Numerical models for the solar cells

Based on the above sensitivity analysis, in the next step, all the essential variables are implemented in the model to quantify the material properties. More performance data is included in the fitting process to reduce the uncertainty of the optimised parameters. In the following, the light J-V curves for four temperatures 300K, 280K, 260K, 240K are added. Temperature-dependent measurements are carried out using a cold finger cryostat mounted on a liquid nitrogen source. The optimised parameters in the models are shown in Table 5. The defects capture cross-sections in the CdS layer have a rather large uncertainty for both S1600 and S1000. Other parameters including doping density, defect properties in the CIGSe layer, absorption model constant A, back barrier, R_s, R_{sh} have an uncertainty $< 20\%$. This result ensures the reliability of the stochastically determined numerical model. The optimised models also have good correspondence with the measurements as shown in Figure 6,7,8.

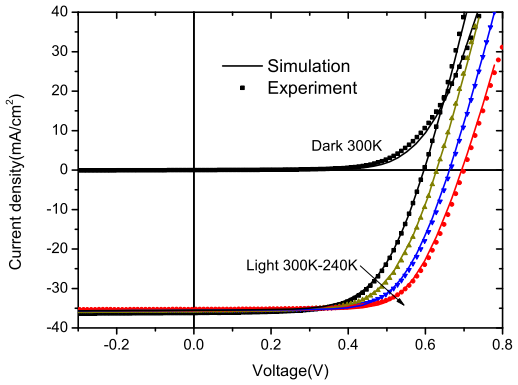

Figure 6: J-V curves of S1600 at 300K, 280K, 260K, 240K: symbols (measurements); lines (fitting using the numerical model)

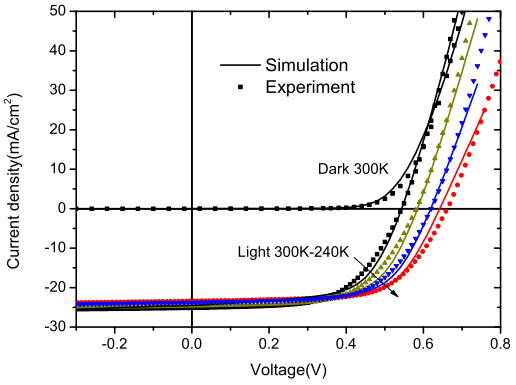

Figure 7: J-V curves of S1000 at 300K, 280K, 260K, 240K: symbols (measurements); lines (fitting using the numerical model)

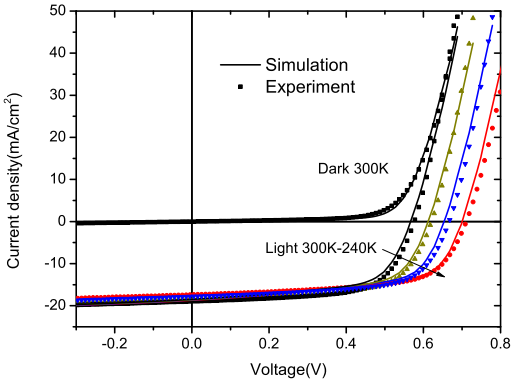

Figure 8: J-V curves of S430 at 300K, 280K, 260K, 240K: symbols (measurements); lines (fitting using the numerical model)

5. Discussion

5.1. Absorption coefficient of CIGSe layer

As shown in Table 5, the absorption coefficient for the CIGSe absorber layer in all the 3 solar cells is lower than the well-known value 10^5cm^{-1}. The absorption of 10^5 cm^{-1} for CIGSe absorber layer has been questioned[49, 50, 51], a lower value in the range of 10^4 cm^{-1} is found by spectroscopic ellipsometry (SE) and the high α reported in previous studies is attributed to the transmission loss induced by the strong surface light scattering [52]. On the other hand, the absorption coefficient in the presented model is linked directly to the generated electron-hole pairs, but in the reality, there are several losses for the absorption: the shading by top contact coverage, shading by the measurement needles, reflection from the front and back surface. Thus the light generated electron-hole pairs are less than expected.

5.2. Recombination mechanism

Deep level defects are observed in samples S1600 and S1000. From the four regression tests for S1600, it is found that the presence of defects in the bulk of the CIGSe absorber layer represents the major recombination mechanism in S1600. Based on the further optimised model of sample S1600 with parameters shown in Table 5, the influence of the defects on the S1600 cell performance is studied. The defects in the CIGSe absorber layer are found to be deep defects that have a rather large capture cross-section for holes thus will reduce the carrier lifetime for holes significantly. In

S1600, a negative back barrier for holes is found. The reason for the negative barrier could be that accumulated Ga at the back contact forms a bandgap grading and introduces a back surface field(BSF) that reduces the bulk/back surface recombination. With this negative back barrier and a good carrier collection at the back contact, both the minority and the majority carrier lifetime become important for solar cell efficiency. As shown in Figure 9, curve 1 is the light IV curve at 300K based on the original model. Curve 2 shows the light IV curve at 300K when removing the observed bulk defects in CIGSe layer in the model. After moving the defects in the bulk of the CIGSe layer, the efficiency of the solar cell increases from 13.33% to 16.15%.

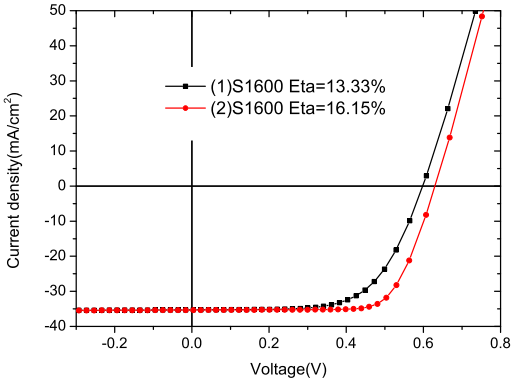

Figure 9: Light IV curves for S1600: (1)S1600 calculated with the optimised model; (2)S1600 calculated with removing the bulk defects of CIGSe layer in the model.

The influence of defects in S1000 is investigated as well. The light IV curve at 300K with removing the CIGSe bulk defects in the model is plotted in Figure 10 (curve 2), curve 1 is the one with the optimised model. Comparing curve 1 and curve 2, the defects in the bulk of the CIGSe layer do not significantly deteriorate the solar cell performance. However, in S1000 and S430, the recombination at the back contact is found to be the main loss mechanism. As shown in Figure 10 (curves 3) and Figure 11 (curves 2), these two curves are calculated by introducing a negative back barrier(-0.2eV) in both cells S1000 and S430. A negative barrier reduces the recombination current at the back contact. With the reduced recombination at the back contact, the efficiency in sample S430 increases to 11.09% and the efficiency in sample S1000 increases to 16.67%. The deterioration effect of back contact recombination on ultra-thin CIGSe solar cells performance confirms the work of Touafek et al.[53]. The CIGSe absorber layer of S1000 and S430 are all made by one stage co-evaporation. The thickness of S430 also has a limitation on the cell's efficiency. From the simulation, we found that the efficiency of S430 can be further increased to 15.78% by increasing the thickness of the absorber to 1μm. Curve 3 in Figure 11 is calculated based on the model for curve 2 but for an absorber thickness 1μm.

5.3. Doping profiles

The doping profiles of the three samples derived from the CV measurement(measured at a frequency f=100kHz) is shown in Figure 12. S1600 shows a higher doping density in the optimised model than the one derived from CV measurement. The reason can be that both free holes and charges in the traps respond in the CV measurement which leads to an overestimation for the free carriers [54]. In S1000, the minimum point of the doping profile from CV measurements is lower than the one derived from modelling but both of them indicate a doping density in the order of $10^{15}cm^{-3}$. In S430, the minimum point of the doping profile from CV measurements corresponds well with the fitting results. S430 shows a higher doping density than S1000 and that could due to the KF treatment[21]. In S1000 and S430, the measured depletion width is close to the absorber thickness, this is an indication of a fully depleted CIGSe absorber layer. The fully depleted absorber leads to a good carrier collection ability so that the defects have limited influence on the solar cell performance. This could be the reason that defects are not found to be the main efficiency limiting factor in ultra-thin solar cells S1000 and S430.

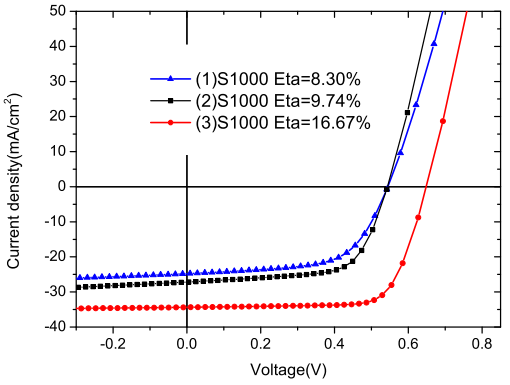

Figure 10: Light IV curves for S1000: (1)S1000 calculated with the optimised model; (2)S1000 calculated with removing the bulk defects of CIGSe layer in the model; (3)S1000 calculated with removing the bulk defects and changing the barrier at the back contact to -0.2eV

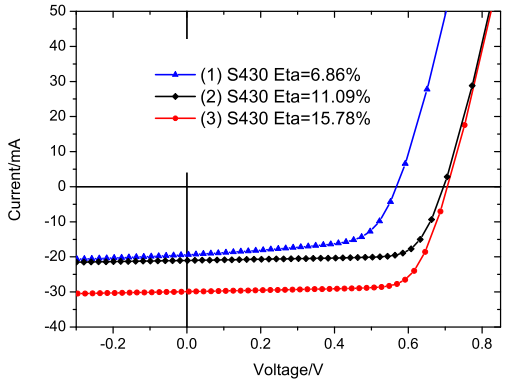

Figure 11: Light IV curves for S430: (1)S430 calculated with the optimised model; (2)S430 calculated with changing the barrier at the back contact to -0.2eV. (3)S430 calculated with changing the barrier at the back contact to -0.2eV and increase the thickness to 1um.

6. Conclusion

Recombination mechanisms are verified in three CIGSe solar cells using regression analysis with numerical modelling based on the solar cell performance. Numerical models are proposed for the three solar cells as well. From the analysis of the proposed model, for S430 and S1000 with relatively thin CIGSe absorber layers prepared using a one-stage evaporation, the main loss mechanism is the back surface recombination. In S1600 prepared using a two-step process with a rather thick absorber and a good carriers collection at the back contact, the cell performance is found to be limited by deep defects decreasing the holes lifetime in the CIGSe absorber and therefore the V_{oc}. Based on the modelling results, information is provided to the solar cell manufacturers to improve the CIGSe solar cell performance: For ultra-thin CIGSe solar cells with poor carrier collection at the back contact interface, the problem to solve first is to reduce the surface recombination at the back contact. For a solar cell with good carrier collection ability at the back contact, reducing deep level defects in the bulk of the CIGSe absorber is important for increasing the solar cell efficiency.

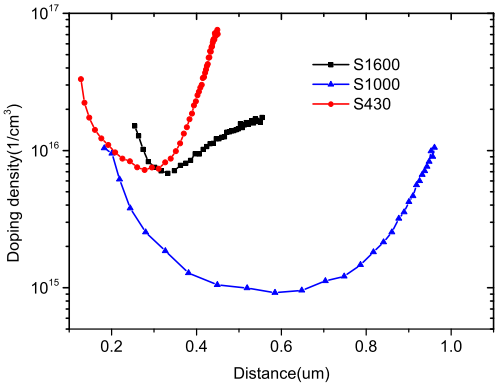

Figure 12: The doping profile of the CIGSe layer derived from CV measurements(measured at f=100kHZ) in the three samples S1600, S1000 and S430

Acknowledgement

This work is supported by the Special Research Fund (BOFSTA201600501) of Ghent University.

References

[1] Martin Green, Ewan Dunlop, Jochen Hohl-Ebinger, Masahiro Yoshita, Nikos Kopidakis, and Xiaojing Hao. Solar cell efficiency tables (version 57). *Progress in Photovoltaics: Research and Applications*.

[2] T Walter, R Herberholz, C Müller, and HW Schock. Determination of defect distributions from admittance measurements and application to Cu(In,Ga)Se_2 based heterojunctions. *Journal of Applied Physics*, 80(8):4411–4420, 1996.

[3] DV Lang. Deep-level transient spectroscopy: A new method to characterize traps in semiconductors. *Journal of applied physics*, 45(7):3023–3032, 1974.

[4] R Herberholz, M Igalson, and HW Schock. Distinction between bulk and interface states in $CuInSe_2$/CdS/ZnO by space charge spectroscopy. *Journal of Applied Physics*, 83(1):318–325, 1998.

[5] Jennifer T Heath, J David Cohen, and William N Shafarman. Bulk and metastable defects in $CuIn_{1-x}Ga_xSe_2$ thin films using drive-level capacitance profiling. *Journal of Applied Physics*, 95(3):1000–1010, 2004.

[6] Tobias Eisenbarth, Thomas Unold, Raquel Caballero, Christian A Kaufmann, and Hans-Werner Schock. Interpretation of admittance, capacitance-voltage, and current-voltage signatures in Cu(In,Ga)Se_2 thin film solar cells. *Journal of Applied Physics*, 107(3):034509, 2010.

[7] Johan Lauwaert, Jeroen Lauwaert, Lisanne Van Puyvelde, Joris W Thybaut, and Henk Vrielinck. Modeling of capacitance transients of thin-film solar cells: A valuable tool to gain information on perturbing layers or interfaces. *Applied Physics Letters*, 104(5):053502, 2014.

[8] K Wiśniewski, A Urbaniak, and P Zabierowski. Exploration of the two-diode model of deep level transient spectroscopy signal originating from secondary barriers. *Thin Solid Films*, 674:76–81, 2019.

[9] Susanne Siebentritt. What limits the efficiency of chalcopyrite solar cells? *Solar Energy Materials and Solar Cells*, 95(6):1471–1476, 2011.

[10] G Hanna, A Jasenek, U Rau, and HW Schock. Open circuit voltage limitations in $CuIn_{1-x}Ga_xSe_2$ thin-film solar cells–dependence on alloy composition. *physica status solidi (a)*, 179(1):R7–R8, 2000.

[11] A Krysztopa, M Igalson, L Gütay, Jes K Larsen, and Y Aida. Defect level signatures in $CuInSe_2$ by photocurrent and capacitance spectroscopy. *Thin Solid Films*, 535:366–370, 2013.

[12] Jacopo Parravicini, Maurizio Acciarri, Matteo Murabito, Alessia Le Donne, Andrea Gasparotto, and Simona Binetti. In-depth photoluminescence spectra of pure CIGS thin films. *Applied optics*, 57(8):1849–1856, 2018.

[13] SB Zhang, Su-Huai Wei, Alex Zunger, and H Katayama-Yoshida. Defect physics of the $CuInSe_2$ chalcopyrite semiconductor. *Physical Review B*, 57(16):9642, 1998.

[14] Su-Huai Wei, SB Zhang, and Alex Zunger. Effects of Ga addition to $CuInSe_2$ on its electronic, structural, and defect properties. *Applied physics letters*, 72(24):3199–3201, 1998.

[15] Laura Oikkonen et al. Atomic-scale defects in solar cell material $CuInSe_2$ from hybrid-functional calculations. 2013.

[16] Johan Pohl and Karsten Albe. Intrinsic point defects in $CuInSe_2$ and $CuGaSe_2$ as seen via screened-exchange hybrid density functional theory. *Physical Review B*, 87(24):245203, 2013.

[17] Jonas Bekaert, Rolando Saniz, Bart Partoens, and Dirk Lamoen. Native point defects in $CuGa_x$ $In_{1-x}Se_2$: hybrid density functional calculations predict the origin of p-and n-type conductivity. *Physical Chemistry Chemical Physics*, 16(40):22299–22308, 2014.

[18] R Saniz, J Bekaert, B Partoens, and D Lamoen. Structural and electronic properties of defects at grain boundaries in $CuInSe_2$. *Physical Chemistry Chemical Physics*, 19(22):14770–14780, 2017.

[19] R Saniz, J Bekaert, B Partoens, and D Lamoen. First-principles study of defects at Σ3 grain boundaries in CuGaSe2. *Solid State Communications*, 330:114263, 2021.

[20] A Bauknecht, S Siebentritt, A Gerhard, W Harneit, S Brehme, J Albert, S Rushworth, and M Ch Lux-Steiner. Defects in $CuGaSe_2$ thin films grown by MOCVD. *Thin Solid Films*, 361:426–431, 2000.

[21] J De Wild, M Simor, DG Buldu, T Kohl, G Brammertz, M Meuris, J Poortmans, and B Vermang. Alkali treatment for single-stage co-evaporated thin cuin0. 7ga0. 3se2 solar cells. *Thin Solid Films*, 671:44–48, 2019.

[22] Shigeru Niki, Miguel Contreras, Ingrid Repins, Michael Powalla, Katsumi Kushiya, Shogo Ishizuka, and Koji Matsubara. CIGS absorbers and processes. *Progress in Photovoltaics: Research and Applications*, 18(6):453–466, 2010.

[23] Chia-Hua Huang, Wen-Jie Chuang, Chun-Ping Lin, Yueh-Lin Jan, and Yu-Chiu Shih. Deposition technologies of high-efficiency CIGS solar cells: development of two-step and co-evaporation processes. *Crystals*, 8(7):296, 2018.

[24] Rui Kamada, William N Shafarman, and Robert W Birkmire. Cu (In, Ga) Se_2 film formation from selenization of mixed metal/metal–selenide precursors. *Solar Energy Materials and Solar Cells*, 94(3):451–456, 2010.

[25] Timo Jäger, Yaroslav E Romanyuk, Benjamin Bissig, Fabian Pianezzi, Shiro Nishiwaki, Patrick Reinhard, Jérôme Steinhauser, Johannes Schwenk, and Ayodhya N Tiwari. Improved open-circuit voltage in Cu (In, Ga) Se_2 solar cells with high work function transparent electrodes. *Journal of Applied Physics*, 117(22):225303, 2015.

[26] Sudhanshu Shukla, Damilola Adeleye, Mohit Sood, Florian Ehre, Alberto Lomuscio, Thomas Paul Weiss, Daniel Siopa, Michele Melchiorre, and Susanne Siebentritt. Carrier recombination mechanism and photovoltage deficit in 1.7-eV band gap near-stoichiometric Cu (In, Ga) S_2. *Physical Review Materials*, 5(5):055403, 2021.

[27] Simon Min Sze. *Semiconductor devices: physics and technology*. John wiley & sons, 2008.

[28] Markus Gloeckler, Caroline R Jenkins, and James R Sites. Explanation of light/dark superposition failure in CIGS solar cells. *MRS Online Proceedings Library Archive*, 763, 2003.

[29] Marie Buffière, Guy Brammertz, Souhaib Oueslati, Hossam El Anzeery, J Bekaert, K Ben Messaoud, C Köble, Samira Khelifi, Marc Meuris, and Jef Poortmans. Spectral current–voltage analysis of kesterite solar cells. *Journal of Physics D: Applied Physics*, 47(17):175101, 2014.

[30] Marc Burgelman, Peter Nollet, and Stefaan Degrave. Modelling polycrystalline semiconductor solar cells. *Thin Solid Films*, 361:527–532, 2000.

[31] Paul A Basore, DT Rover, and AW Smith. PC-1D version 2: Enhanced numerical solar cell modelling. In *Conference Record of the Twentieth IEEE Photovoltaic Specialists Conference*, pages 389–396. IEEE, 1988.

[32] JA Rodriguez, P Otero, M Vetter, J Andreu, E Comesana, and AJ Garcia-Loureiro. Simulation of the effect of p-layer properties on the electrical behaviour of a-Si: H thin film solar cells. In *Proceedings of the 8th Spanish Conference on Electron Devices, CDE'2011*, pages 1–4. IEEE, 2011.

[33] Sheng Yang, Samira Khelifi, Guy Brammertz, Leo Choubrac, Nicolas Barreau, Pieter Bolt, Bart Vermang, and Johan Lauwaert. Numerical modelling of the performance-limiting factors in CZGSe solar cells. *Journal of Physics D: Applied Physics*, 53(38):385102, 2020.

[34] H Gajewski and K Gärtner. On the iterative solution of van roosbroeck's equations. *ZAMM-Journal of Applied Mathematics and Mechanics/Zeitschrift für Angewandte Mathematik und Mechanik*, 72(1):19–28, 1992.

[35] Khairy Sayed, Mazen Abdel-Salam, Mahmoud Ahmed, and Adel A Ahmed. Numerical Simulation of Thin-Film Photovoltaic Solar Cells. In *ASME International Mechanical Engineering Congress and Exposition*, volume 54907, pages 1127–1134, 2011.

[36] Patricio Farrell, Nella Rotundo, Duy Hai Doan, Markus Kantner, Jürgen Fuhrmann, and Thomas Koprucki. Numerical methods for drift-diffusion models. 2016.

[37] Antonino Parisi, Luciano Curcio, Vincenzo Rocca, Salvatore Stivala, Alfonso C Cino, Alessandro C Busacca, Giovanni Cipriani, Diego La Cascia, Vincenzo Di Dio, Rosario Miceli, et al. Thin film CIGS solar cells, photovoltaic modules, and the problems of modeling. *International Journal of Photoenergy*, 2013, 2013.

[38] Jeff Bailey, Geordie Zapalac, and Dmitry Poplavskyy. Metastable defect measurement from capacitance-voltage and admittance measurements in Cu(In,Ga)Se_2 solar cells. In *2016 IEEE 43rd Photovoltaic Specialists Conference (PVSC)*, pages 2135–2140. IEEE, 2016.

[39] Michal Cwil, Małgorzata Igalson, Paweł Zabierowski, and Susanne Siebentritt. Charge and doping distributions by capacitance profiling in Cu(In,Ga)Se_2 solar cells. *Journal of Applied Physics*, 103(6):063701, 2008.

[40] Marco Nardone, Yasas Patikirige, Curtis Walkons, Shubhra Bansal, Theresa M Friedlmeier, Kyoung E Kweon, Joel B Varley, and Vincenzo Lordi. Baseline models for three types of CIGS cells: Effects of buffer layer and na content. In *2018 IEEE 7th World Conference on Photovoltaic Energy Conversion (WCPEC)(A Joint Conference of 45th IEEE PVSC, 28th PVSEC & 34th EU PVSEC)*, pages 3013–3018. IEEE, 2018.

[41] Florian Werner, Tobias Bertram, Jonathan Mengozzi, and Susanne Siebentritt. What is the dopant concentration in polycrystalline thin-film Cu(In,Ga)Se_2. *Thin Solid Films*, 633:222–226, 2017.

[42] PK Paull, J Bailey, G Zapalac, and AR Arehart. Fast cv method to mitigate effects of deep levels in cigs doping profiles. In *2017 IEEE 44th Photovoltaic Specialist Conference (PVSC)*, pages 2414–2418. IEEE, 2017.

[43] Xiaocheng Yang, Chunchuan Xu, and NC Giles. Intrinsic electron mobilities in CdSe, CdS, ZnO, and ZnS and their use in analysis of temperature-dependent Hall measurements. *Journal of Applied Physics*, 104(7):073727, 2008.

[44] M Gloeckler, AL Fahrenbruch, and JR Sites. Numerical modeling of CIGS and CdTe solar cells: setting the baseline. In *3rd World Conference onPhotovoltaic Energy Conversion, 2003. Proceedings of*, volume 1, pages 491–494. IEEE, 2003.

[45] Rainer Storn and Kenneth Price. Differential evolution–a simple and efficient heuristic for global optimization over continuous spaces. *Journal of global optimization*, 11(4):341–359, 1997.

[46] Kashif Ishaque, Zainal Salam, Saad Mekhilef, and Amir Shamsudin. Parameter extraction of solar photovoltaic modules using penalty-based differential evolution. *Applied Energy*, 99:297–308, 2012.

[47] Leonardo Dagum and Ramesh Menon. OpenMP: An industry-standard API for shared-memory programming. *Computing in Science & Engineering*, 5(1):46–55, 1998.

[48] AO Pudov, A Kanevce, HA Al-Thani, JR Sites, and FS Hasoon. Secondary barriers in CdS-$CuIn_{1-x}Ga_xSe_2$ solar cells. *Journal of applied*

physics, 97(6):064901, 2005.

[49] María Isabel Alonso, Miquel Garriga, CA Durante Rincón, Elvis Hernández, and Máximo León. Optical functions of chalcopyrite $CuGa_x In_{1-x}Se_2$ alloys. *Applied Physics A*, 74(5):659–664, 2002.

[50] Shota Minoura, Takuji Maekawa, Keita Kodera, Akihiro Nakane, Shigeru Niki, and Hiroyuki Fujiwara. Optical constants of Cu (In, Ga) Se_2 for arbitrary Cu and Ga compositions. *Journal of Applied Physics*, 117(19):195703, 2015.

[51] Romain Carron, Enrico Avancini, Thomas Feurer, Benjamin Bissig, Paolo A Losio, Renato Figi, Claudia Schreiner, Melanie Bürki, Emilie Bourgeois, Zdenek Remes, et al. Refractive indices of layers and optical simulations of Cu (In, Ga) Se_2 solar cells. *Science and Technology of advanced MaTerialS*, 19(1):396–410, 2018.

[52] Shota Minoura, Keita Kodera, Takuji Maekawa, Kenichi Miyazaki, Shigeru Niki, and Hiroyuki Fujiwara. Dielectric function of Cu(In,Ga)Se_2-based polycrystalline materials. *Journal of Applied Physics*, 113(6):063505, 2013.

[53] Naima Touafek and R Mahamadi. Back surface recombination effect on the ultra-thin CIGS solar cells by SCAPS. *International Journal of Renewable Energy Research (IJRER)*, 4(4):958–964, 2014.

[54] Augustin McEvoy, Tom Markvart, Luis Castañer, T Markvart, and Luis Castaner. *Practical handbook of photovoltaics: fundamentals and applications*. Elsevier, 2003.